Electronic Supplementary Material (ESI) for Physical Chemistry Chemical Physics.

Supporting Information: Isothermal relaxation kinetics for the reduction and oxidation of $SrFeO_3$ based perovskites.

Brendan Bulfin[a,*], Josua Vieten[b,c], Sebastian Richter[b,c], Madhusudhan J. Naik[d], Greta R. Patzke[d], Martin Roeb[b], Christian Sattler[b,c], Aldo Steinfeld[a]

[a] Department of Mechanical and Process Engineering, ETH Zürich, 8092 Zürich, Switzerland; [b] Institute of Solar Research, German Aerospace Center, 51147 Cologne; [c] Faculty of Mechanical Science and Engineering, Institute of Power Engineering, Professorship of Solar Fuel production, TU Dresden, 01062 Dresden, Germany [d] Department of Chemistry, University of Zurich, Winterthurerstrasse 190, CH-8057 Zurich, Switzerland;

Tel: +41 44 633 87 30; E-mail: bulfin@ethz.ch

Contents

1 XRD Analysis

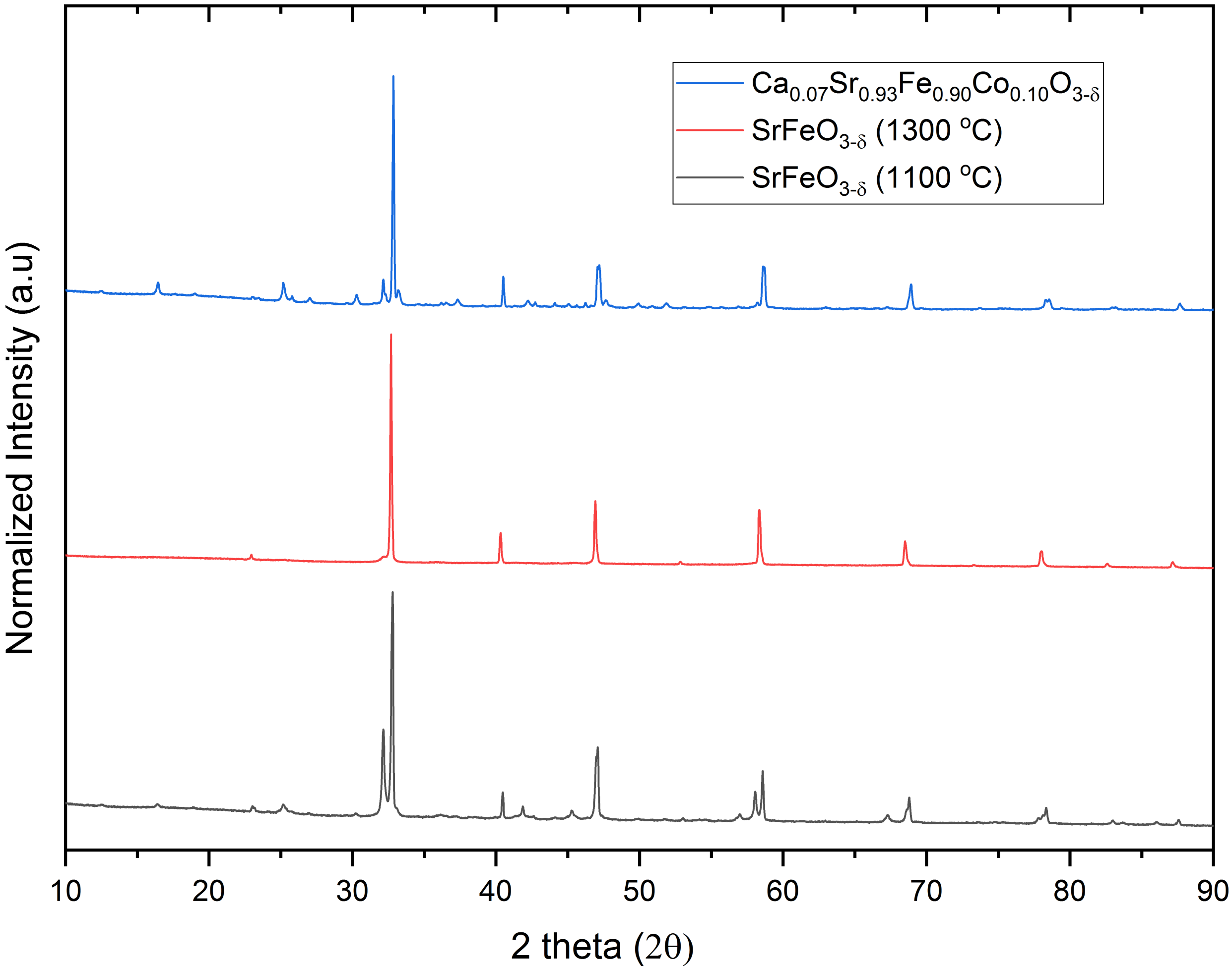

Figure 1: XRD patterns of the three samples, the $SrFeO_3$ powder produced via a solid state route with annealing at 1100 °C, the ground pellet which was produced from this powder and annealed at 1300 °C, and the SCFCO sample synthesized via the Pechini method with annealing at 1300 °C. The $SrFeO_3$ sample annealed at 1300 °C shows a pure cubic perovskite structure. The $SrFeO_3$ powder sample and the SCFCO sample both contain some extents of secondary phases, which are oxygen deficient tetragonal perovskite phases.

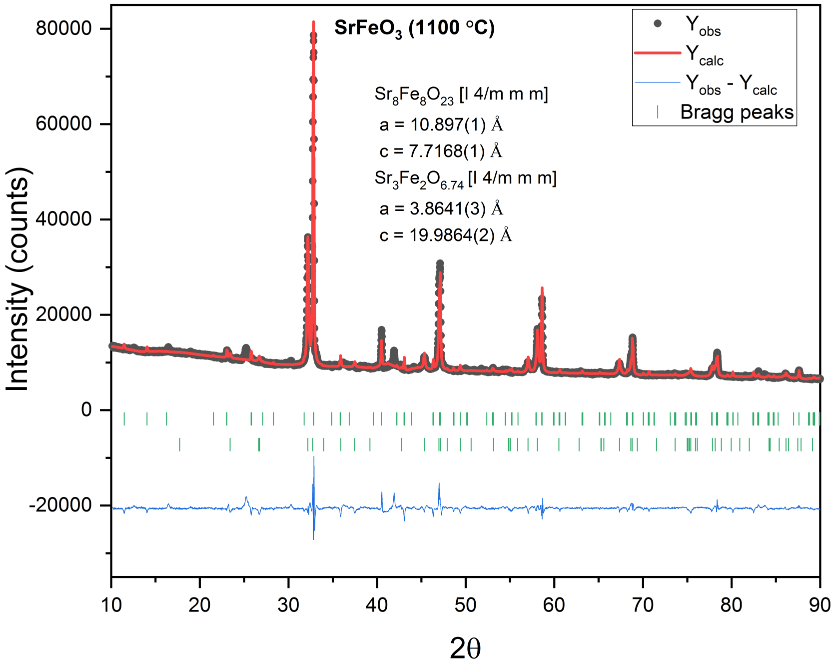

Figure 2: Refinement of the XRD pattern of the $SrFeO_3$ powder sample, which shows two distinct tetragonal phases, with details given in table 2.

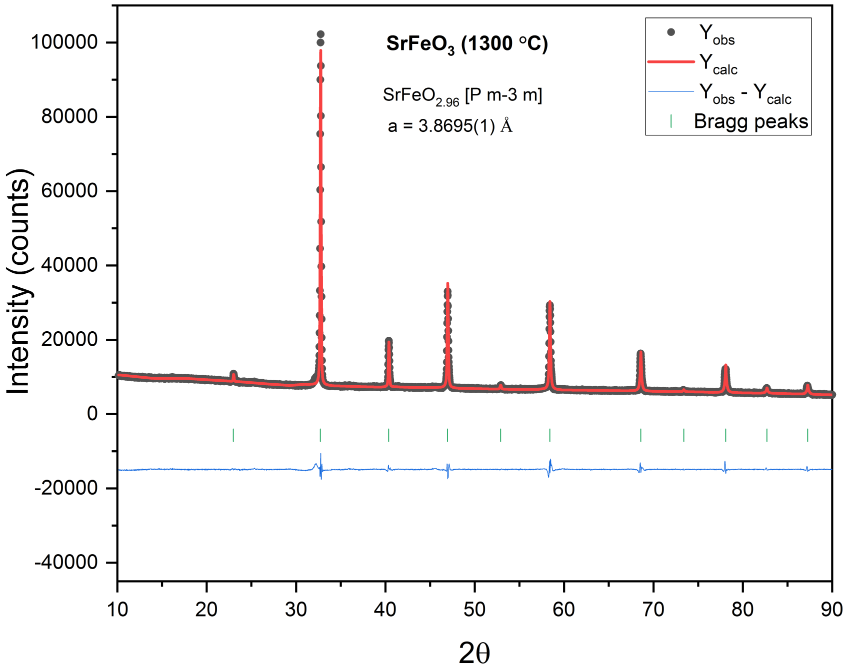

Figure 3: Refinement of the XRD pattern of the $SrFeO_3$ ground pellet, which matches with the cubic perovskite structure. See results of the fit in table 2.

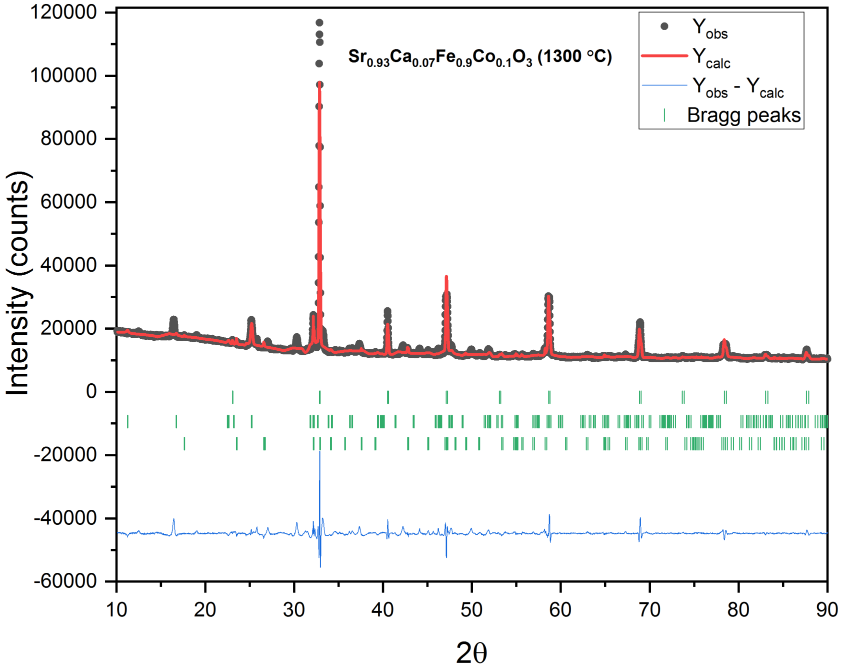

Figure 4: Refinement of the XRD pattern of the SCFCO powder sample, where the most distinct phase was again the cubic perovskite structure.

The cif file used to fit the data of the cubic phases was that of $SrFeO_{2.96}$,[1] which had a lattice parameter of $a = 3.8531$. The refinement for the pellet sample gave a larger lattice parameter of $a = 3.8695$ (table 2) which is likely due to the fact that we expect there to be larger oxygen non-stoicheometry (c.a. $SrFeO_{2.85}$ or lower), which would result in a lattice expansion as more iron will be in the Fe^{3+} state which has a larger atomic radius. In the case of SCFCO the cubic lattice parameter was $a = 3.85432$, which is smaller than that of the $SrFeO_3$ cubic perovskite seen for the pellet. This small shrinkage in the lattice parameter for SCFCO can be attributed to the smaller ionic radii of $Co^{3+/4+}$ and Ca^{2+} relative to $Fe^{3+/4+}$ and Sr^{2+}. The other phases seen for SCFCO sample are a brownmillerite and layered perovskite.

Table 1: Results obtained from a Rietveld fit of XRD data.

Sample	cif	space group	wt %	cif lattice parameters	fit lattice parameters	fit Chi^2
			±2 %	[Å]	[Å]	
$SrFeO_3$ powder	$Sr_8Fe_8O_{23}$ [2]	$I4mmm$	50 %	$a = 10.9317$	$a = 10.8970(7)$	16.1
				$c = 7.7009$	$c = 7.7170(5)$	
1100 °C	$Sr_3Fe_2O_{6.74}$ [3]	$I4mmm$	50 %	$a = 3.8642$	$a = 3.8641(3)$	
				$c = 20.05010$	$c = 19.986(2)$	
$SrFeO_3$ pellet	$SrFeO_{2.96}$[1]	$Pm\bar{3}m$	100 %	$a = 3.8531$	$a = 3.8695(1)$	4.14
SCFCO	$SrFeO_{2.96}$[1]	$Pm\bar{3}m$	80 %	$a = 3.8531$	$a = 3.8543(1)$	28.5
	$Sr_2Fe_{1.9}Co_{0.1}O_5$ † [4]	$Icmm$	10 %	$a = 5.62436$	$a = 5.624(3)$	
				$c = 15.5963$	$b = 15.707(9)$	
				$c = 5.51770$	$c = 5.558(2)$	
	$Sr_3FeCoO_{5.425}$ [5]	$I4mmm$	10 %	$a = 3.8786$	$a = 3.8497(1)$	
				$c = 20.309$	$c = 20.116(1)$	

† A brownmillerite structure, which is a reduced perovskite, $A_2B_2O_5$.

2 SEM of powders.

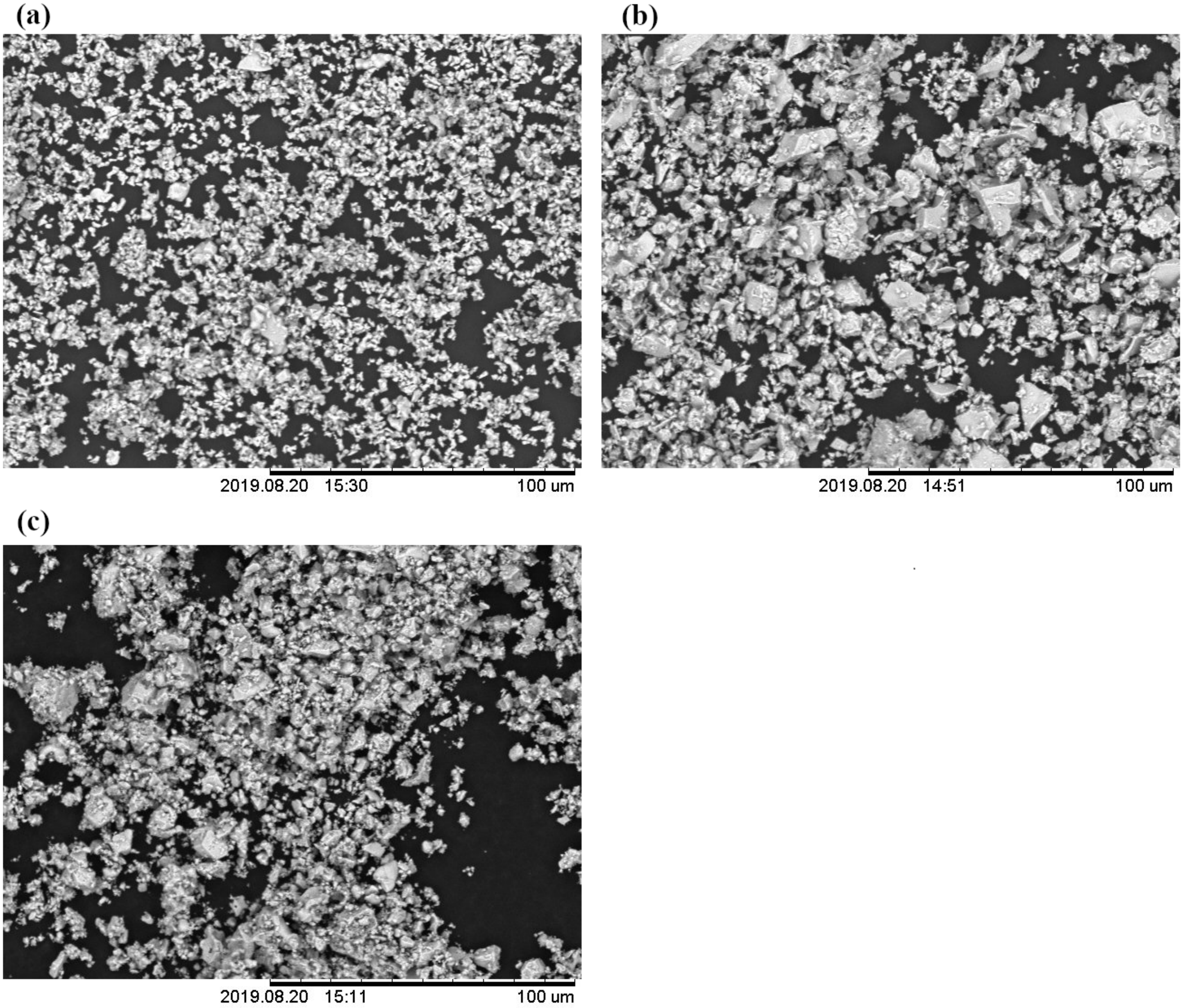

Figure 5: SEM images of the powder sample used to visually confirm size distribution measurements in the laser flash system. **(a)** $SrFeO_3$ powder synthesized via a solid state route with sintering at 1373 K. **(b)** The pellet sintered at 1573 K, after it was ground back into a powder. **(c)**
SCFCO powder synthesized via Pechini method with sintering at 1573 K. See table 1 in the manuscript, for results of particle size distribution.

3 TGA raw data

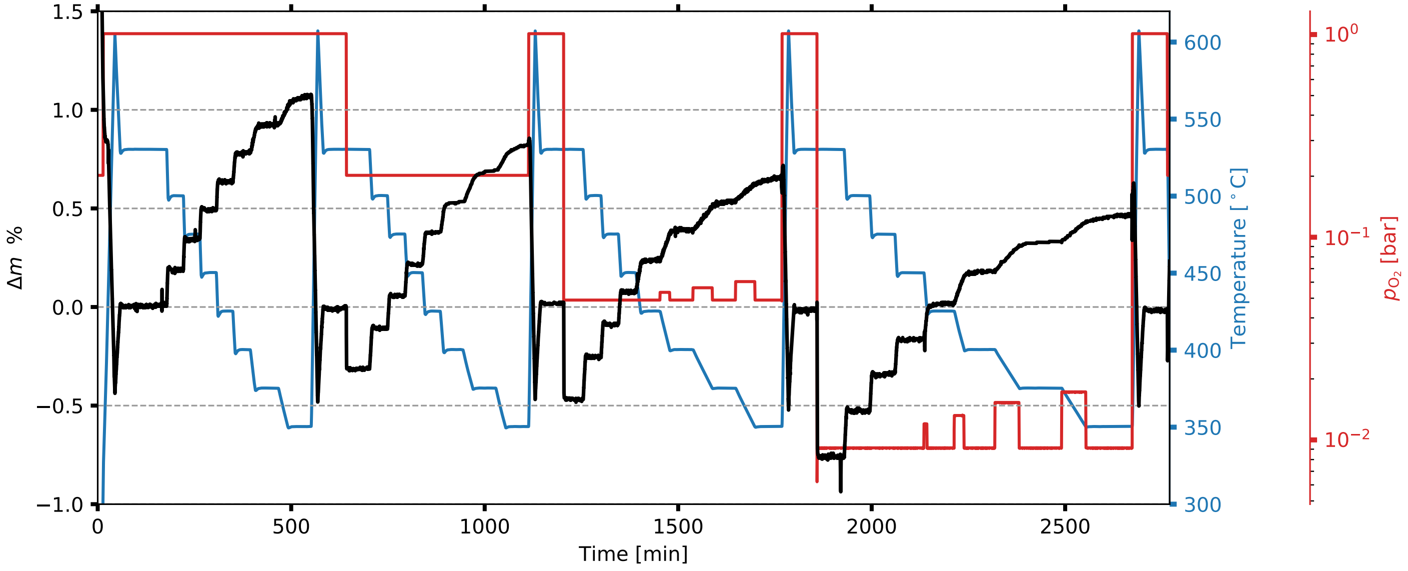

Figure 6: The TGA dataset used to collect the equilibrium data for $SrFeO_3$. The areas where the temperature, the oxygen partial pressure and the mass plateau, were taken as the equilibrium points which are plotted in figure 2 of the main paper.

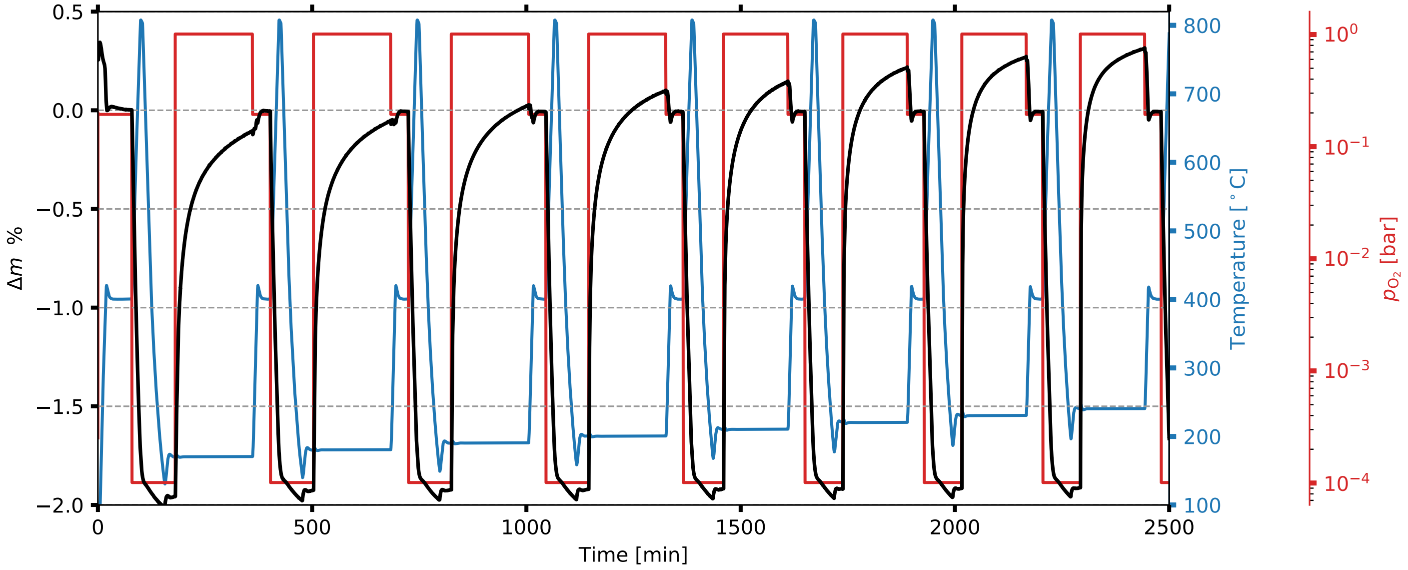

Figure 7: A sample TGA dataset of oxidation kinetics for the $SrFeO_3$ pellet. Samples are heated to high temperature under argon, then cooled to the desired oxidation temperature. Once the temperature is stabilized a flow of pure oxygen is fed to the TGA causing re-oxidation of the sample.

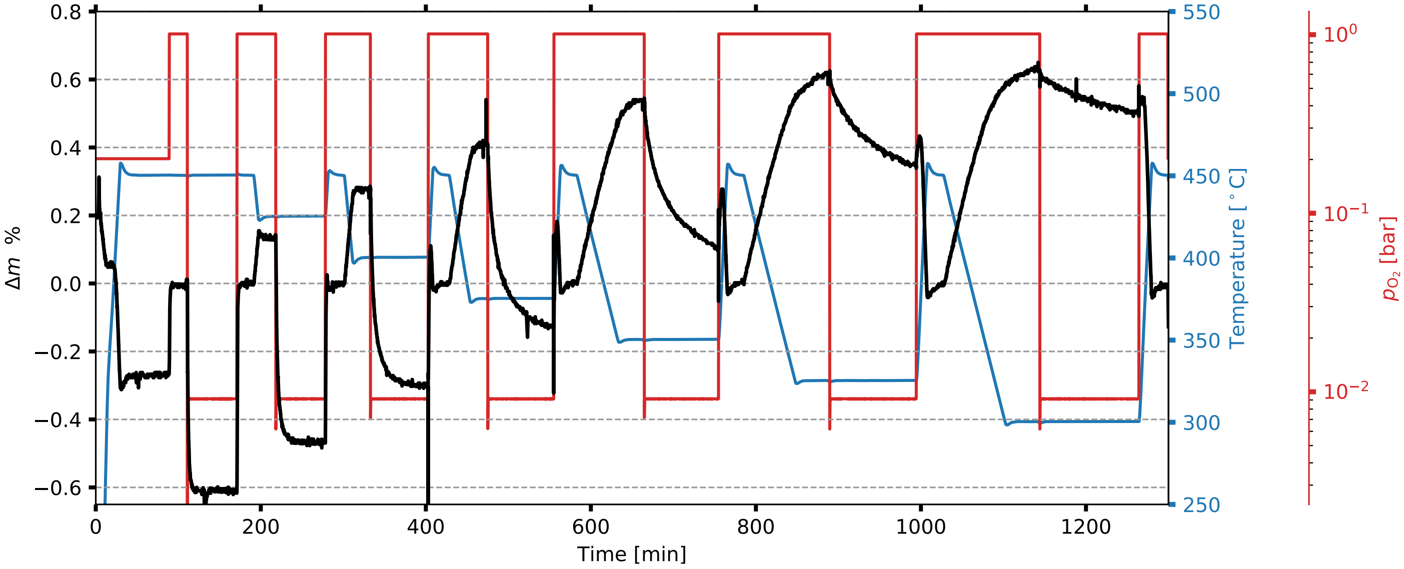

Figure 8: The TGA dataset from the reduction kinetics experiments of $SrFeO_3$. At isothermal conditions the gas is switched from pure oxygen to a 1% oxygen atmosphere, and sample starts loosing mass reduction of the sample.

4 Equilibrium extrapolation

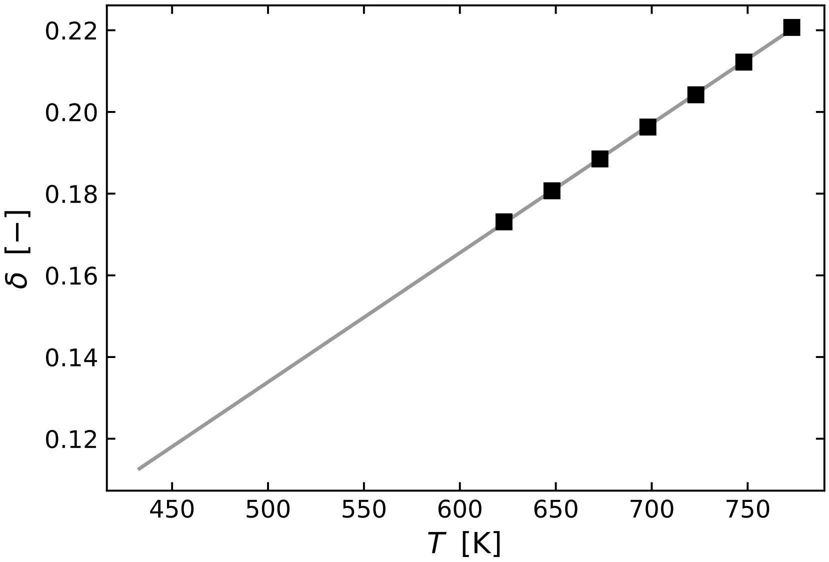

Figure 9: A graph showing the linear extrapolation δ vs. T used to determine the end points of the oxidation reactions for $SrFeO_3$. In this case the partial pressure was of was 1 bar oxygen. The data is plotted in terms of absolute δ where it is important that we do not reach $\delta = 0$, as at this point the dependence would be expected to change.

5 Gas switching times

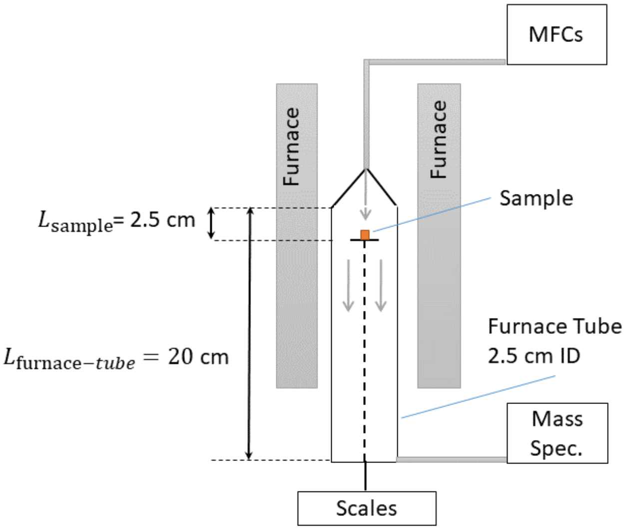

Figure 10: The TGA setup used to perform the thermal analysis, gases are fed from the MFC's into the furnace tube. Down stream of the furnace is a mass spectrometer used to analyse switching times.

Figure 10 shows a schematic of the TGA system used for the kinetic analysis. To quantify the gas switching time it is important to consider the time required for the mass flow to switch $t_{\text{MFC}-\text{switch}} = 3\,\text{s}$, and diffusion along the flow.

The tubes leading to and from the TGA furnace have an inner diameter of 0.4 cm and for a flow rate of 100 $\text{ml}\,\text{min}^{-1}$ at s.t.p. a flow velocity of $u \approx \frac{\dot{V}}{A} = 13\,\text{cm}\,\text{s}^{-1}$. The tubes are approximately 100 cm in length and diffusion along the flow is negligible in this section due to the high Péclet number.

However, for gas in the furnace tube the larger diameter results in a much slower flow velocity. At 473 K ($u \propto T$), the velocity in the larger furnace tube is $u \approx \frac{\dot{V}}{A} = 0.5\,\text{cm}\,\text{s}^{-1}$. For the gas interface to cover the distance to the sample ($L_{\text{Sample}} = 3\,\text{cm}$, where 0.5 cm has been added on to approximate the cone section) we then require a time $\Delta t = \frac{L_{\text{Sample}}}{u} = 6\text{s}$. The characteristic diffusion length along the furnace in this time is given by $L_d = \sqrt{4D\Delta t}$. At this temperature the diffusion coefficient for oxygen in Argon is $D = 1.12$,[6], and the characteristic diffusion length is $L_d = 4.63cm^{-1}$. This means the gas switch interface has spread over approximately $2L_d$ along the length of the furnace. We therefore estimate the gas switching time to be given by,

$$t_{\text{switch}} = t_{\text{MFC}-\text{switch}} + \frac{2L_d}{u}. \tag{1}$$

This time is ment approximate the time required for the sample to see the gas switch start and then reach 90 % complete, or that we have 90 % oxygen at the sample. We can repeat this calculation for the apparent gas switching time measured at the mass spectrometer by replaceing L_{Sample} with $L_{\text{Furnace}-\text{tube}}$ as the gas switching interface has more time to spread out down stream of the sample.

Table 2: The gas switching time t_{switch} in seconds calculated at the sample, at the mass-spectrometer (MS) and the time measured at the mass-spectrometer for the oxygen to go from zero to 90%, or drop to 10 % for reduction. The switching times at both the upper and lower temperatures in the range of analysed data were calculated, but only measured at the upper temperature.

	Flow rate	$t_{\text{switch}-\text{sample}}$	$t_{\text{switch}-\text{MS}}$	$t_{\text{switch}-\text{MS}}$ measured
Oxidation 553 K	100 ml/min	20 s	46 s	50±2 s
Oxidation 453 K	100 ml/min	22 s	52 s	-
Reduction 723 K	200 ml/min	7 s	15 s	12±2 s
Reduction 723 K	200 ml/min	8 s	17 s	- s

6 Oxidation Kinetics

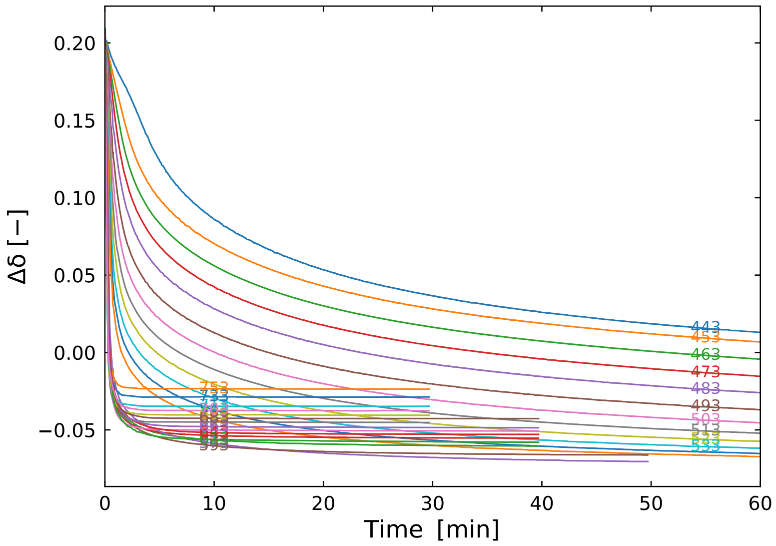

Figure 11: The relative change in non-stoicheometry $\Delta\delta$ vs. time for the $SrFeO_3$ pellet. This data was used to extract $t_{1/2}$ and to determine the conversion extent X.

6.1 Isoconversional analysis

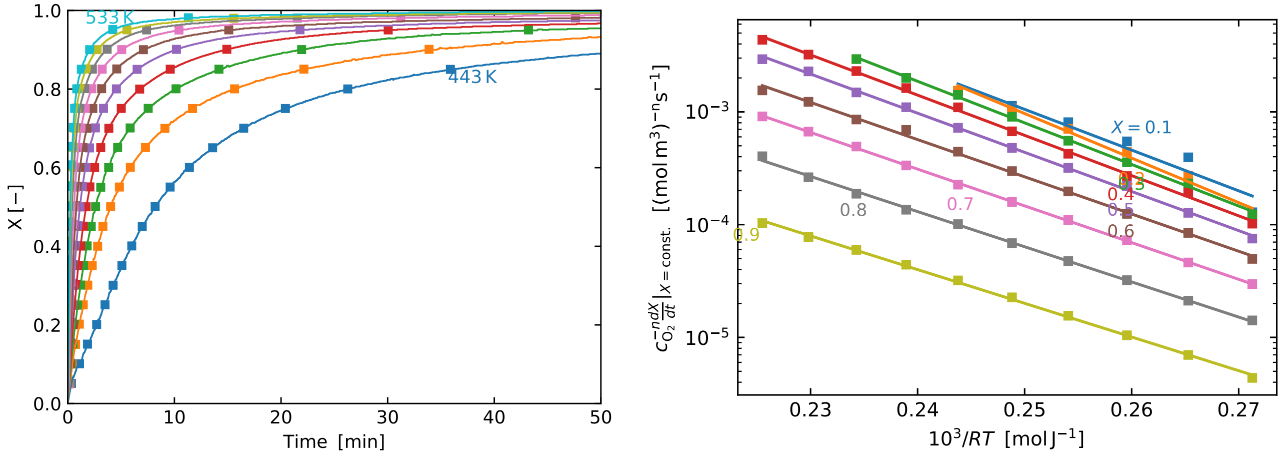

Figure 12: Experimental data for SCFCO. **Left:** Conversion extent X vs. time for temperatures in the range 443-543 K in steps of 10 K. **Right:** $c_{O_2}^{-n}\frac{dX}{dt}\Big|_{X=\text{const.}}$ plotted on a log scale vs. $\frac{10^3}{RT}$ where the slope of each line is the activation $-E_a$ in [kJ mol^{-1}], which are given in table 2 of the manuscript.

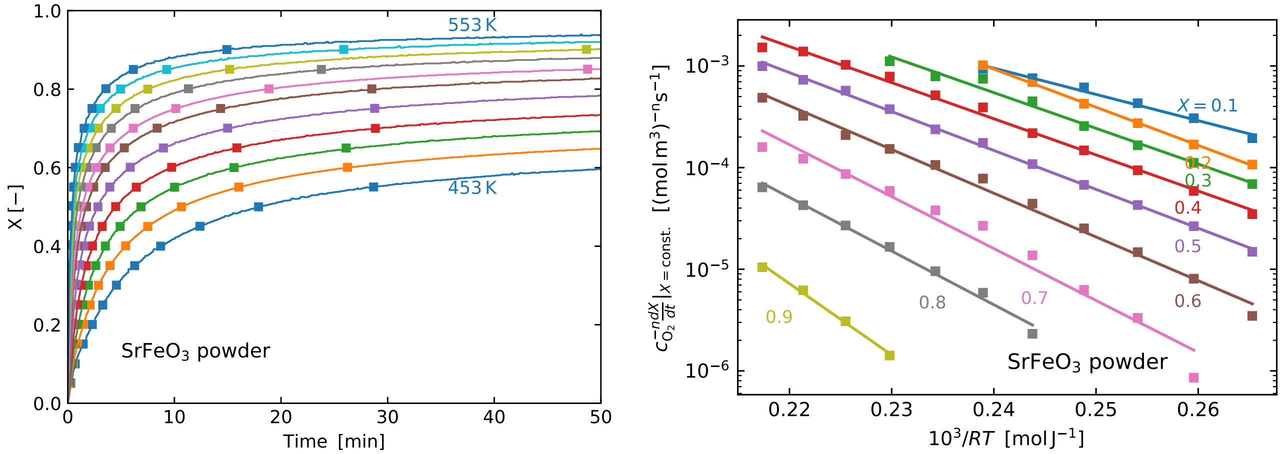

Figure 13: Experimental data for SrFeO$_3$ powder sample annealed at 1373 K. **Left:** Conversion extent X vs. time for temperatures in the range 453-553 K in steps of 10 K. **Right:** $c_{O_2}^{-n}\frac{dX}{dt}\Big|_{X=\text{const.}}$ plotted on a log scale vs. $\frac{10^3}{RT}$ where the slope of each line is the activation $-E_a$ in [kJ mol^{-1}], which are given in table 2 of the manuscript. Comparison to figure 12 above it can be seen that SCFCO has a greater reaction rate.

6.2 Model fitting

Here we show the fits of a simple power law model to the experimental data according to the equation,

$$\frac{dX}{dt} = \left(\frac{dX}{dt}\right)_{t=0} (1-X)^m \tag{2}$$

where the initial rate is given by,

$$\left(\frac{dX}{dt}\right)_{t=0} = c_{\mathrm{O}_2}^n k_0 \exp\left(\frac{E_a}{RT}\right) \tag{3}$$

taking the logarithm of both sides gives,

$$\log\left(\frac{dX}{dt}\right) = m\log(1-X) + \log\left(\left(\frac{dX}{dt}\right)_{t=0}\right) \tag{4}$$

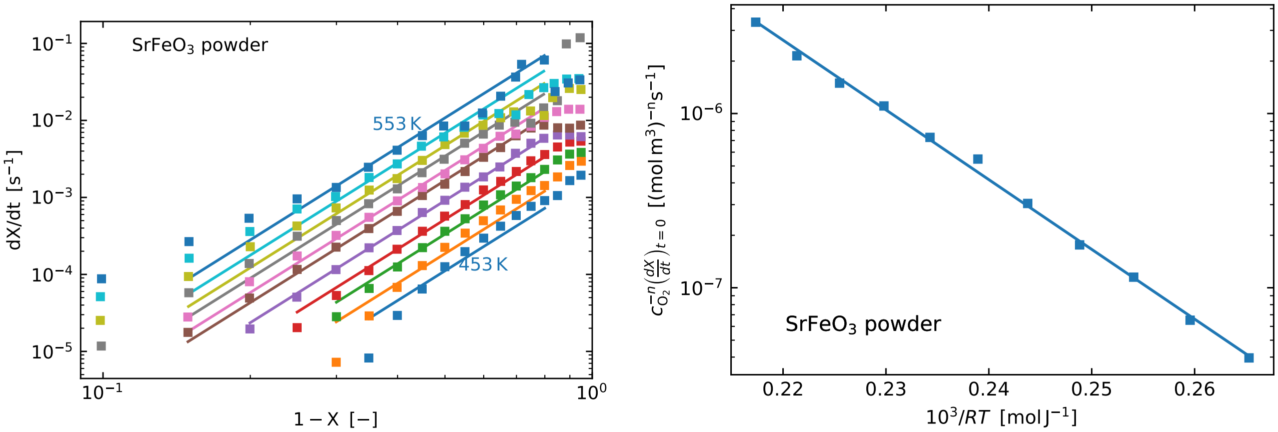

Figure 14: Model fitting for the $\mathrm{SrFeO_3}$ powder sample annealed at 1373 K. **Left:** $\frac{dX}{dt}$ vs. $1-X$ with a log-log scale. The markers show the experimental data from figure 13. The lines show a fit of equation 2. **Right:** A plot of $c_{\mathrm{O}_2}^{-n}\left(\frac{dX}{dt}\right)_{t=0}$ vs. $\frac{10^3}{RT}$ using the intercepts form the model fits on the left. The log scale data is then fit linearly, which according to equation 3, gives the activation energy as the slope E_a, and preexponetial factor as the intercept $\log(k_0)$. The resulting values are given in table 2 of the manuscript.

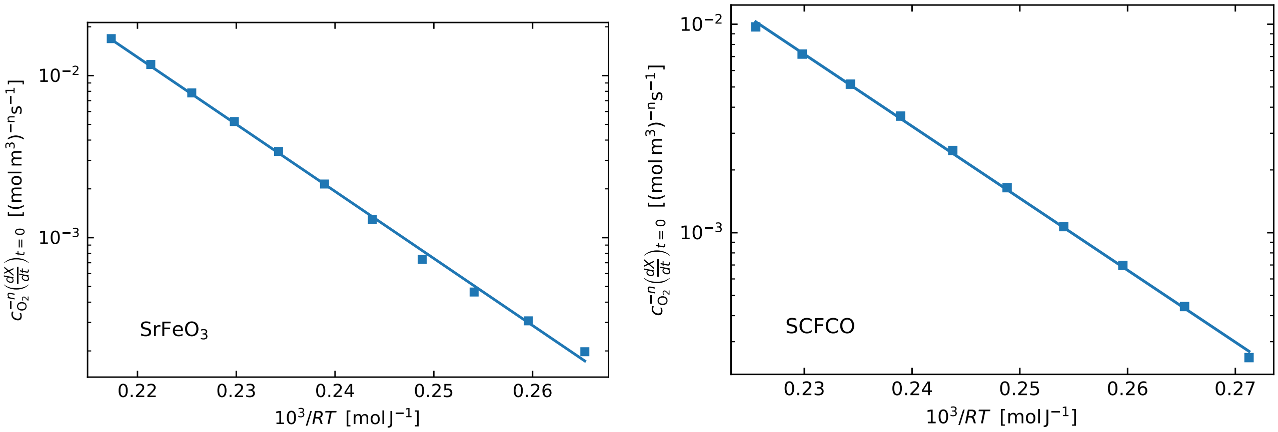

Figure 15: Plots of $c_{\mathrm{O}_2}^{-n}\left(\frac{dX}{dt}\right)_{t=0}$ vs. $\frac{10^3}{RT}$ using the intercepts from figure 5 of the manuscript. The straight line fits are used to determine the activation energy E_a (slope), and pre-exponential $\log(k_0)$ (intercept) according to equation 3. **Left:** $\mathrm{SrFeO_3}$ pellet. . **Right:** SCFCO powder.

7 Reduction Kinetics

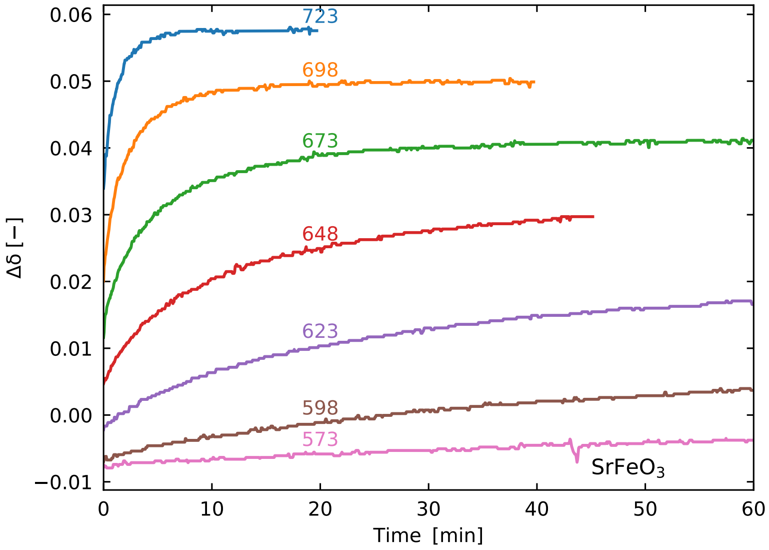

Figure 16: The relative change in non-stoicheometry $\Delta\delta$ vs. time for the $SrFeO_3$ ground pellet during reduction relaxation experiments. This data was used to extract $t_{1/2}$ and to determine the conversion extent X.

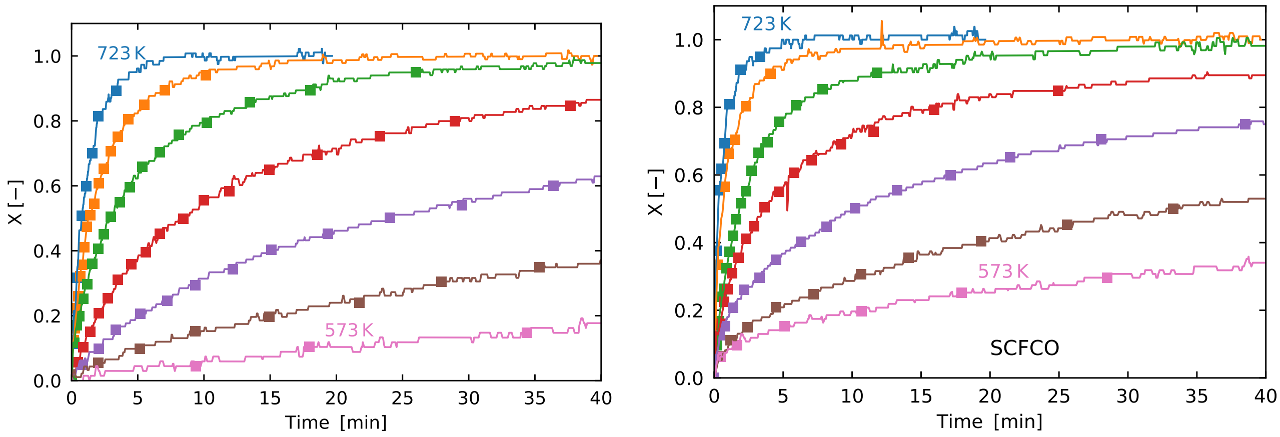

Figure 17: Plots of the conversion extent vs. time for the reduction relaxation kinetics of the $SrFeO_3$ ground pellet (left), and the SCFCO sample (right).

7.1 Isoconversional analysis

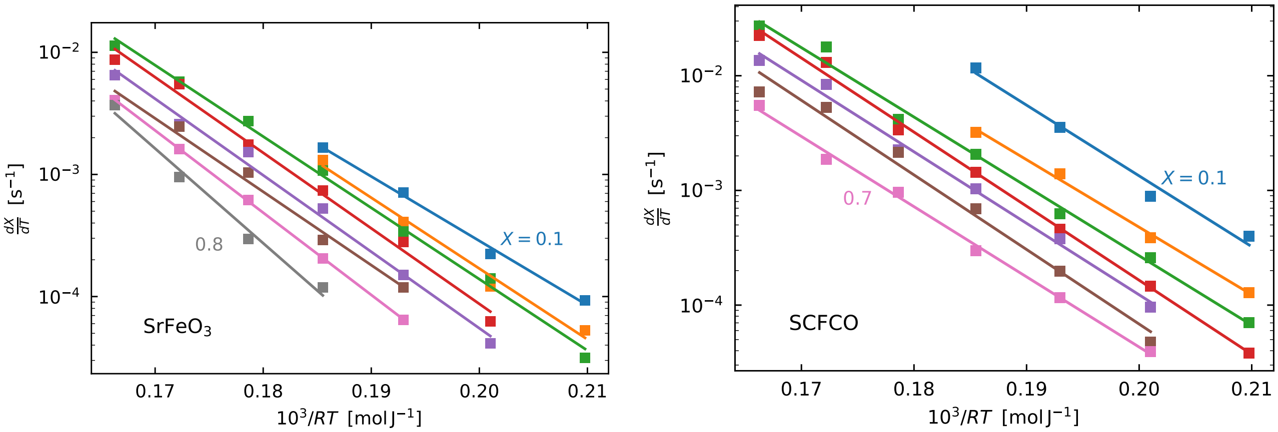

Figure 18: The isoconversional method applied to the reduction relaxation kinetics, with $\left.\frac{dX}{dt}\right|_{X=\text{const.}}$ plotted on a log scale vs. $\frac{10^3}{RT}$ where the slope of each line is the activation $-E_a$ in [kJ mol^{-1}], which are given in table 3 of the manuscript. On the left is the data for the $SrFeO_3$ ground pellet, and on the right the SCFCO sample.

7.2 Model fitting

Again using the basic power law of equation 2, but with the initial rate now given by,

$$\left(\frac{dX}{dt}\right)_{t=0} = k_0 \exp\left(\frac{E_a}{RT}\right). \tag{5}$$

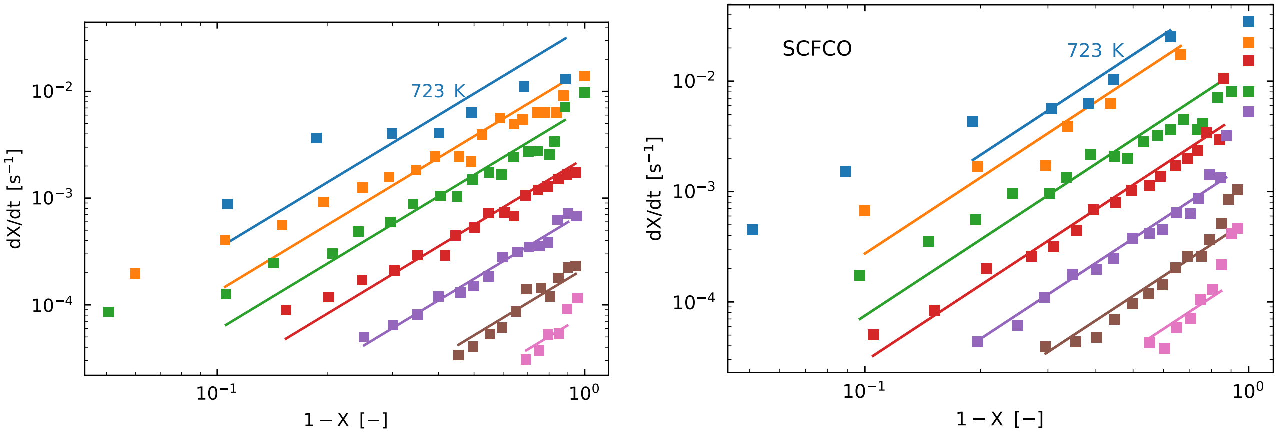

Figure 19: $\frac{dX}{dt}$ vs. $1 - X$ with a log-log scale. The markers show the experimental data from figure 18, and The lines show a fit of equation 2, where the slopes are the paramater m. On the left is the data for the $SrFeO_3$ ground pellet, and on the right the SCFCO sample.

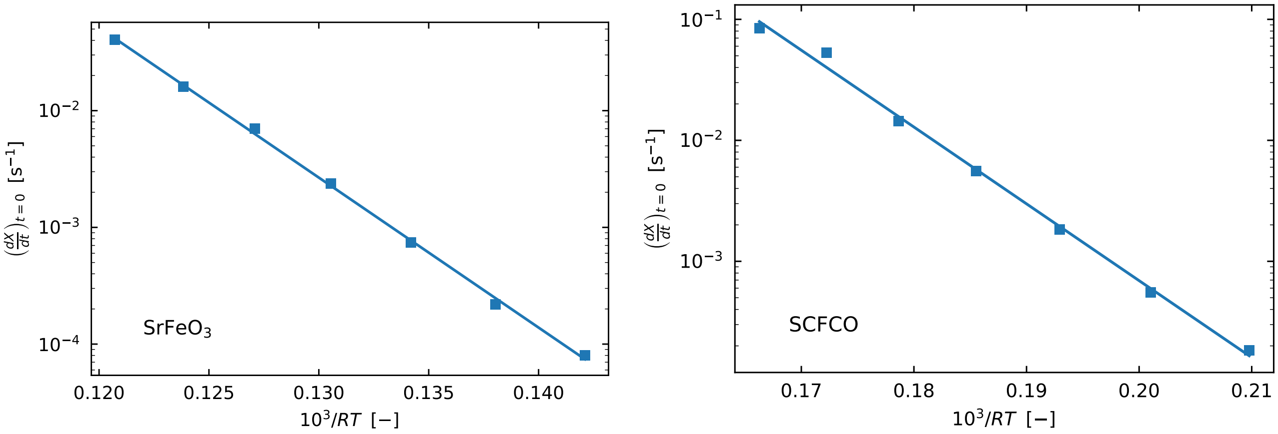

Figure 20: Plots of $\left(\frac{dX}{dt}\right)_{t=0}$ vs. $\frac{10^3}{RT}$ using the intercepts from figure of the manuscript. The straight line fits are used to determine the activation energy E_a (slope), and pre-exponential $\log(k_0)$ (intercept) according to equation 5. On the left is the data for the $SrFeO_3$ ground pellet, and on the right the SCFCO sample.

References

[1] Javier Blasco, Jolanta Stankiewicz, and Joaquín García. Phase segregation in the $\mathrm{Gd}_{1-x}\mathrm{Sr}_x\mathrm{FeO}_{3-\delta}$ series. *Journal of Solid State Chemistry*, 179(3):898–908, 2006.

[2] F Deganello, LF Liotta, A Longo, MP Casaletto, and M Scopelliti. Cerium effect on the phase structure, phase stability and redox properties of Ce-doped strontium ferrates. *Journal of Solid State Chemistry*, 179(11):3406–3419, 2006.

[3] SE Dann, MT Weller, and DB Currie. Structure and oxygen stoichiometry in Sr3Fe2O7-y, 0≤ y ≤ 1.0. *Journal of Solid State Chemistry*, 97(1):179–185, 1992.

[4] Farshid Ramezanipour, John E Greedan, Lachlan MD Cranswick, V Ovidiu Garlea, Joan Siewenie, Graham King, Anna Llobet, and Ronald L Donaberger. The effect of the b-site cation and oxygen stoichiometry on the local and average crystal and magnetic structures of $\mathrm{Sr}_2\mathrm{Fe}_{1.9}\mathrm{M}_{0.1}\mathrm{O}_{5+y}$ (M= Mn, Cr, Co; y= 0, 0.5). *Journal of Materials Chemistry*, 22(19):9522–9538, 2012.

[5] Y Bréard, C Michel, M Hervieu, F Studer, A Maignan, and BB Raveau. Large oxygen deficiency in a n= 2 member of the rp series: $\mathrm{Sr}_3\mathrm{FeCoO}_{7-x}$ (x= 1.55). *Chemistry of materials*, 14(7):3128–3135, 2002.

[6] Edward Lansing Cussler and Edward Lansing Cussler. *Diffusion: mass transfer in fluid systems*. Cambridge university press, 2009.